Journal of Sensor Science and Technology
Vol. 31, No. 4 (2022) pp. 218-227
http://dx.doi.org/10.46670/JSST.2022.31.4.218
pISSN 1225-5475/eISSN 2093-7563

Interfacial Material Engineering for Enhancing Triboelectric Nanogenerators

Dinh Cong Nguyen[1] and Dukhyun Choi[1,+]

Abstract

Triboelectric nanogenerators (TENGs), a new green energy, that have various potential applications, such as energy harvesters and self-powered sensors. The output performance of TENGs has been improving rapidly, and their output power significantly increased since they were first reported owing to improved triboelectrification materials and interfacial material engineering. Because the operation of a TENG is based on contact electrification in which electric charges are exchanged at the interface between two materials, its output can be increased by increasing the contact area and charge density. Material surface modification with microstructures or nanostructures has increased the output performance of TENGs significantly because not only does the sharp micro/nano morphology increases the contact area during friction, but it also increases the charge density. Chemical treatment in which ions or functional groups are added has also been used to improve the performance of TENGS by modifying the work functions, charge densities, and dielectric constants of the triboelectric materials. In addition, ultrahigh output power from TENGs without using new materials or treatments has been obtained in many studies in which special structures were designed to control the current release or to collect the charge current directly. In this review, we discuss physical and chemical treatments, bulk modifications, and interfacial engineering for enhancing TENG performance by improving contact electrification and electrostatic induction.

Keywords: Triboelectrification, physical treatments, chemical treatments, embedded impurities, interfacial layers

1. INTRODUCTION

The triboelectric nanogenerator (TENG) is a simple, efficient, cost-effective, environmentally friendly, and new energy technology harvester, that can convert several forms of mechanical energy into electrical power [1-5]. Many studies have demonstrated the potential of large-scale energy harvesting from natural sources, such as the wind [6,7], rain[7], and ocean waves [8], to complement and replace fossil fuels. Moreover, owing to their high sensitivity and linearity, TENGs can be used as temperature [9], vibration [10], motion [11,12], humidity [13], pressure [14], gas [15], and self-powered sensors[16]. Their flexibility has led to proposals for using TENGs in wearable electronic networks formed by billions of devices in which each device contributes microwatts to milliwatts of power [17,18].

In recent years, the output performance of TENGs has increased rapidly to over 100 MW/m^2 through a variety of strategies, such as the use of triboelectric materials, friction surface nano/microstructure modification, material doping, and ion-gel/liquid deposition. The impressive ability of a single TENG to power a 180 W lamp is promising for applications in daily living [19]. Challenges in further improvements of TENGs include their working mechanisms, technological classification, material selection and preparation, material electrical properties, integration methodology and structural design, and design for energy conversion.

From the perspective of the fundamental operating mechanisms, the design and selection of suitable materials is expected to increase the output power of TENGs for applications in our daily lives. Suitably modified TENG devices provide new possibilities for next-generation power electronics. In particular, engineered modifications to the applied triboelectric materials is expected to improve their contact area, charge density, and charge work function for high-efficiency harvesting. Increasing the charge density is critical for increasing the output because the output increases quadratically with the surface charge density. By optimizing the surface morphology to maximize the contact area and increase the surface charge density, the output performance of TENGs can be improved by tens to thousands of times. Such micro/nanostructure surface modifications have a wide range of applications in energy harvesters, self-powered sensors,

[1]School of Mechanical Engineering, College of Engineering, Sungkyunkwan University, 2066, Seobu-ro, Jangan-gu, Suwon, Gyeonggi 16419, South Korea
[+]Corresponding author: bred96@skku.edu
(Received: Jun. 30, 2022, Revised: Jul. 23, 2022, Accepted: Jul. 27, 2022)

biomechanical energy harvesters, and biomedical devices.

This review focuses on the performance enhancement strategies of physical modification (surface micro/nanostructure, tunneling electrical properties, and ionic layer design), chemical modification (doping, interfacial materials), and charge boosting. Some emerging mechanisms and applications that are attractive targets for extension in future studies are highlighted. Finally, the challenges, future research directions, and applications of TENGs are discussed. Furthermore, we review articles that are expected to be useful to researchers from different majors such as mechanics, chemistry, physics, and material science.

2. TENG ENHANCEMENT

2.1 Physical Modification

Physical modification is a physical method to increase the output performance of TENGs without adding to or changing their chemical components. The contact area is an important parameter that affects the output performance of TENGs because the two triboelectric materials exchange charges with each other through contact. In general, flat surfaces refer as unknow structure. These features provide only limited effective contact area and charge density on the surface, which significantly reduces the output. Therefore, surfaces with uniform microstructures and nanostructures have been fabricated. The surface morphology differs in scale and shape depending on the fabrication method. Many studies on increasing TENG performance through surface modifications have been reported. Photolithography techniques involving ultraviolet (UV) light are suitable for fabricating microstructures. Although nanostructures can be fabricated using e-beam lithography, the process is complicated, costly, and time-consuming. Dudem et al. reported the fabrication of a nanopillar array on a polydimethylsiloxane (PDMS) surface using nano-porous anodic alumina (NAA) templates produced by aluminum anodization without the need for expensive lithography and dry etching processes. The nanopillar array architecture in the PDMS layers was created using imprint lithography [20]. The resultant TENG performance of the different nanopillar diameters shown in the scanning electron microscopy (SEM) images in Fig. 1a(i) was investigated. The contact area is determined by the nanopillar height and period. The relationship between the contact force (effective/uniaxial stress × contact area) and pillar diameter and period was investigated. The contact force increased with the period as the period increased from 100 to 200 nm and decreased when the period was increased further (Fig. 1a-(ii) and 1a-(iii)). In addition, the effect of the pillars was investigated. The highest voltage output obtained at the optimal diameter of 60 nm and period of 125 nm was twice that obtained from the flat TENG, as shown in Fig. 1a(iv). In another study, Fan et al. investigated transparent and flexible triboelectric nanogenerators (FTNGs) with three different microstructure patterns (lines, cubes, and pyramids). To produce these micropatterns, PDMS was coated on wafer molds fabricated using traditional photolithography techniques, and the light-exposed areas were subsequently etched (Fig. 1b-(i))[21]. The pyramidal pattern produced the highest output efficiency, followed by the cubic, linear, and film patterns in sequence. The improvement in the microstructured films compared to the flat films can be explained by the various advantages conferred by the microstructures during the operation of FTNGs, such as a larger effective triboelectric effect, effective dielectric constant, and dipole moment between the electrodes. Because the effective contact area depended on the microstructure pattern, the maximum output performance was achieved in the pyramidal PDMS pattern, which had the largest contact area and contact force. In particular, the power generation capacities of the PDMS films with pyramidal or cubic structures were improved by 5−6 times compared with that of the flat films (Fig. 1b-(ii) and 1a-(iii)).

To further investigate the effect of nano/microstructures on TENGs, Huang et al. fabricated micro/nanostructure-enhanced TENGs using femtosecond-laser direct writing to create nanostructures on both the triboelectric layer and metal electrode [22]. Stripe and conical micro/nanostructures were fabricated on the Cu film surface and micro-bowl structures on the PDMS surface, as shown in Fig. 1c-(i). The small effective pulse number during the fast laser scanning ablation process resulted in the formation of nanoparticles on the microstructures of the Cu surface. To investigate the output power of TENGs with different micro/nanostructures on the triboelectric layers (electrode and PDMS), five types of TENGs were fabricated. The optimal performance was exhibited by a micro/nanocone structure on the Cu surface and a larger microbowl structure on the PDMS surface (2Cu-2P) (Fig. 1c-(ii)). The voltage was improved by more than 4 times and maximum power by 21 times compared to those of a TENG without nano/microstructures on its surfaces.

Bio-nanowire and bio-nanofiber structures have been widely adopted to improve the output performance of TENGs. Kim et al. demonstrated the good output performance of a silk nanofiber-networked TENG produced using electrospun silk (Fig. 1d(i)) fibroin nanofibers [23]. For comparison, the casted flat-silk TENG shown in the SEM image in Fig. 1d-(ii) was also fabricated. The

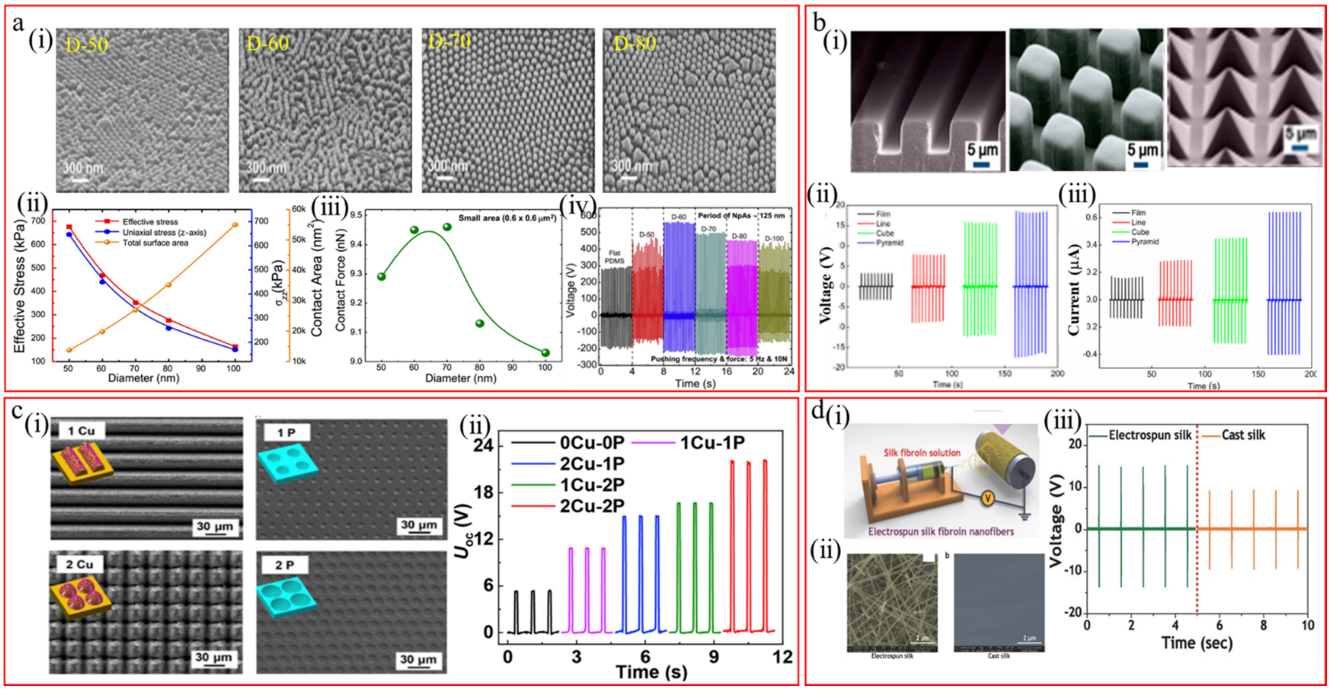

Fig. 1. a- (i) SEM images of nanopillar structures with different diameters of 50, 60, 70, and 80 nm from left to right. Simulation results showing the (ii) effective and uniaxial normal stresses and (iii) contact area as functions of the nanopillar diameter and (iv) variation of TENG output voltage with the PDMS layers. Reprinted with permission from Ref. [20]. b- (i) Three different microstructure patterns: line, cube, and pyramid (scale bar: 5 mm). (ii) Output voltages and (iii) currents from FTNGs fabricated using PDMS thin films with flat surfaces and various patterned features. Reprinted with permission from Ref. [21]. c- TENG with surface morphology modified via direct laser writing: (i) nano/micro cone (1 Cu) and stripe (2 Cu) structures on a Cu substrate and small (1 P) and large micro-bowl (2 P) structures on a PDMS surface. (ii) Output voltage of TENGs with different micro/nanostructures. Reprinted with permission from Ref. [22]. d- (i) Schematic of the electrospun silk fibroin nanofiber-networked film, (ii) FE-SEM images of electrospun and cast silk, and (iii) output voltage of TENGs produced using electrospun and cast silk. Reprinted with permission from Ref. [23].

silk fibers had diameters of 100–200 nm and formed a uniform network. With the same TENG configuration, the silk nanofiber network produced a peak voltage 1.5 times higher than that produced by the cast flat silk (Fig. 1c-(iii)). Enhanced output performance has also been demonstrated in TENGs with nanofiber network structures in other studies [24-27].

In addition to fabricating nanostructures on the surface, another methods to enhance the output performance of TENGs has been demonstrated. Zhu et al. enhanced the output performance of a TENG by depositing a nanoparticle layer on a Au film electrode at an extremely high power density of 313 W/m^2 [28].

2.2 Chemical Modification

Chemical modification involves the use of new surface or chemical components to modify the material electrical properties, such as the surface charge density, dielectric constant, and work function. In this section, we review different modification methods for enhancing the output performance of TENGs.

The type of ion doping is an important consideration for enhancing TENG output. The selected doping material should be appropriate for the base material because bonding to a new form changes the electrical properties of the material. Ba et al. investigated the role of ion doping on the output performance of TENGs by doping cellulose nanofibrils with different ions [29]. Ion doping enhanced the output performance significantly (Fig. 2a-(i)). The optimal output performance was achieved by adding calcium chloride, which resulted in a peak-to-peak voltage and short-circuit current of 254 V and 11.52 μA, respectively (Fig. 2a (ii)). In another study, Lee et al. incorporated 10 wt% of C_{60} into azide-containing polyimide (PI) through a cycloaddition reaction with C_{60} to produce amorphous PI-b-C_{60} with a hydrophobic character. The role of C_{60} in the functionalized PI was investigated. The functionalization resulted in the creation of new energy states that accepted electrons more easily. This resulted in enhanced output performance compared to that of unfunctionalized PI with a 4.3-fold increase in the output power and a 30-fold decrease in the decay rate of the 300 mC m^{-2} charge density generated (Fig. 2a-(iii–v)) [30].

Chemical modifications induced by simple and efficient

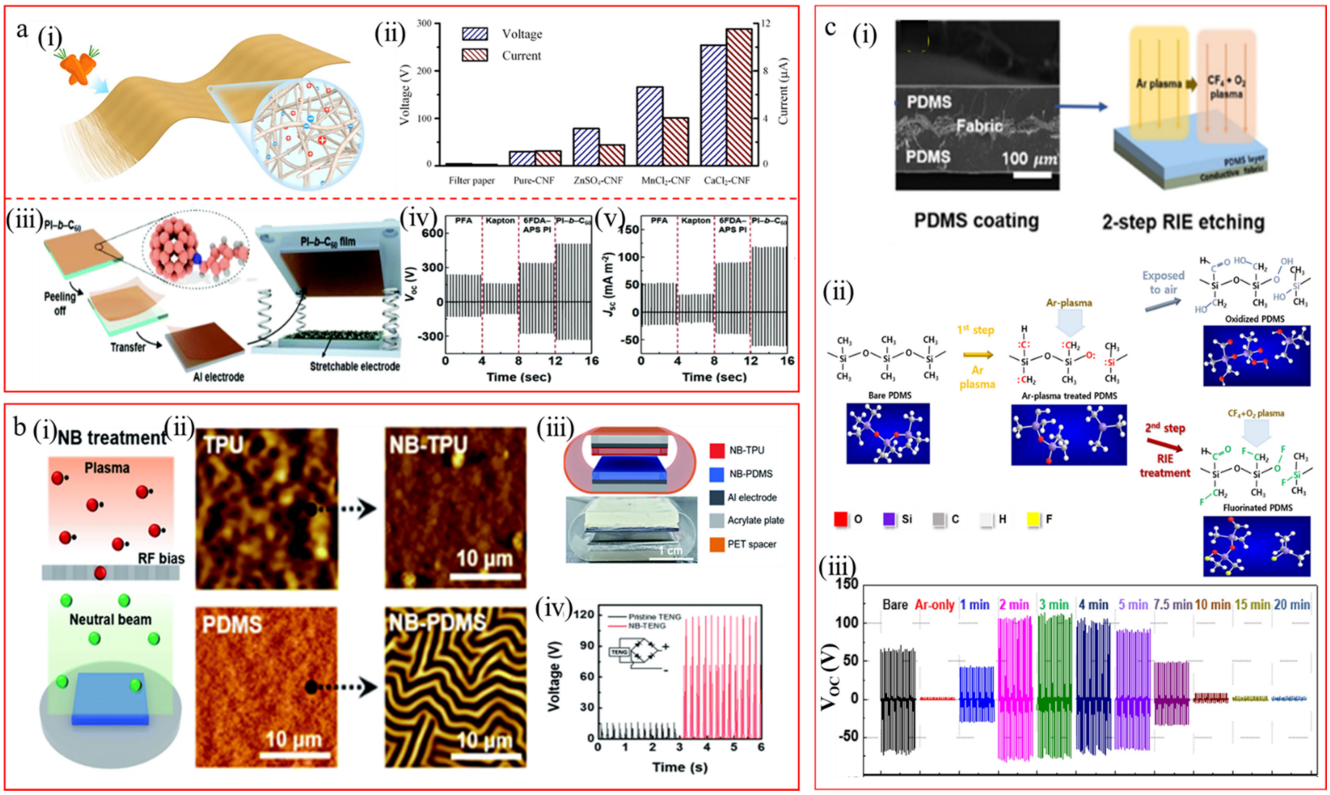

Fig. 2. a- (i) Schematic of cellulose nanofibril paper produced from raw carrot extract and surrounding ions, (ii) output voltage and current of TENGs with different ion doping, (iii) schematic of the fabrication process for the PI-b-C_{60}-based TENG, and (iv) voltage and (v) current density of TENGs with different polymers comprising PFA, Kapton, 6FDA-APS PI, and PI-b-C_{60}. Reprinted with permission from Ref. [29,30]. b- (i) NB treatment process, (ii) AFM images of polymer surfaces before and after the NB treatment of TPU and PDMS, (iii) structure (top) and optical photo (bottom) of NB-treated TENG, and (iv) triboelectric performance of NB-treated TENGs. Reprinted with permission from Ref. [31]. c- (i) Schematic of 2-step RIE etching, (ii) possible mechanisms for the chemical modification of PDMS surfaces via one-step Ar-only plasma treatment and the two-step process with consecutive Ar and CF_4 +O_2 plasmas, which enhanced the triboelectric charging effect, and (iii) output voltage performance of TENGs without the plasma process and TENGs exposed to plasma for different durations. Reprinted with permission from Ref. [35].

physical processes such as high-energy radiation (ultraviolet light, gamma beam, alpha beam, and X-ray) have been studied. Such processes can be used to etch, dope, or/and modify the surface state of materials without defects at the atomic-layer level. Kim et al. used neutral beams to treat PDMS and thermoplastic polyurethane (TPU) that were used as negative and positive triboelectric materials, respectively [31]. A neutral beam (NB) was created using a carbon electrode array to separate the plasma from plasma ions of gaseous N_2 and O_2 (Fig. 2b(i)). In other studies, the surface roughness was increased through NB treatment, which enhanced the TENG performance by increasing the contact area and surface charge density [32-34] (Fig. 2b-(ii)). Although the new bonds (N-relative bonds) created on the PDMS surface (the surface potential of PDMS became relatively positive) could degrade output performance, the increased roughness resulted in improved TENG performance when the NB power was increased. The peak voltage was increased by 6.39 times and the current by 11.37 times compared to those of a pristine TENG (Fig. 2b (iii) and (iv)).

Plasma chemical treatment is a simple method that has been widely used to modify the surfaces of triboelectric materials. Plasma etching is frequently used to create surface nanostructures to increase surface roughness. Ion plasmas of fluorocarbon gases induce fluorinated groups on the surface, which significantly improve the output performance of the TENGs. Fluorocarbon plasma etching is a chemical modification method that involves physical processes. Lee et al. performed a sequential two-step reactive ion plasma treatment with Ar and CF_4 + O_2 plasmas on a PDMS substrate. As shown in Fig. 2c, PDMS was coated onto a fabric film and then subjected to plasma treatment with Ar and CF_4+O_2 (Fig. 2c (i))[35]. The possible mechanisms for the chemical modification of the PDMS surface with only Ar and the two-step Ar and CF_4 + O_2 plasma treatment are shown in Fig. 2c (ii). The Ar plasma broke the weak molecular chains on the

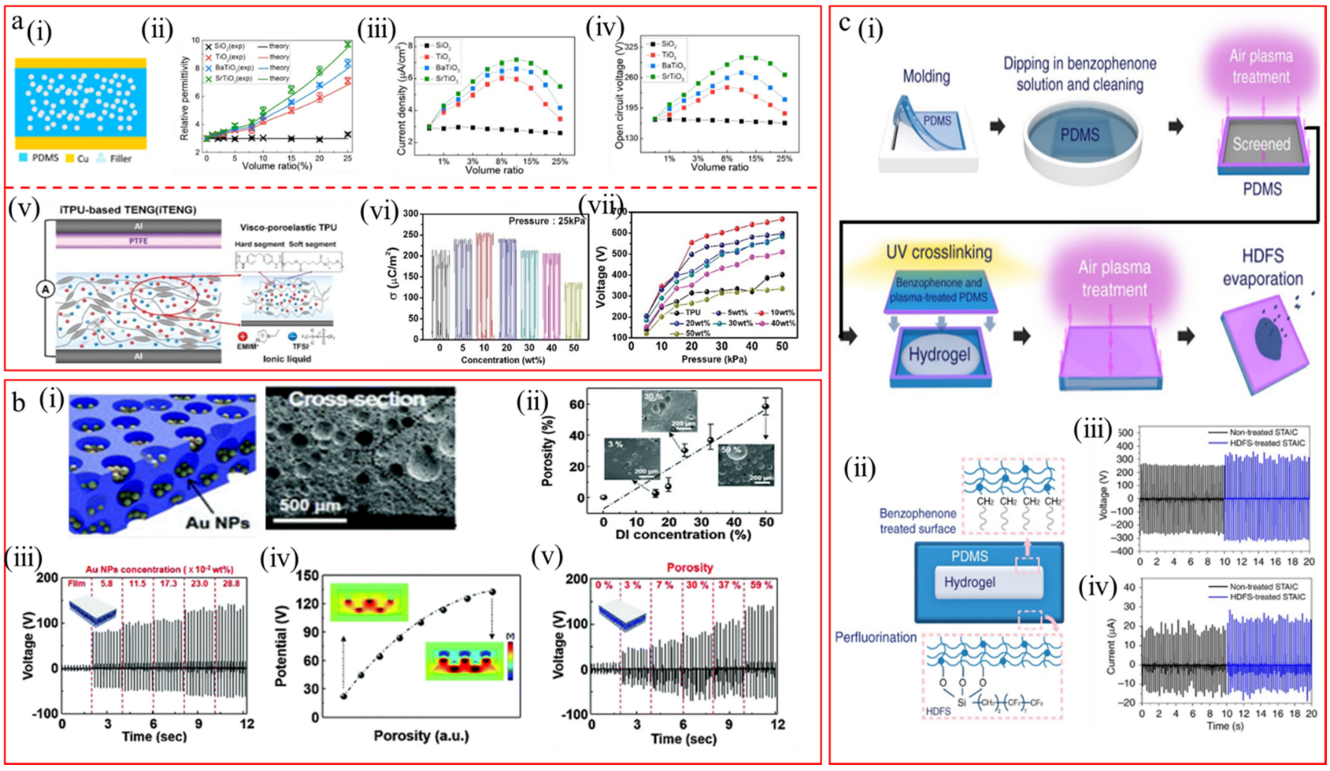

Fig. 3. a- (i)- Illustration of the dielectric material/PDMS composite film and (ii) relative permittivity, (iii) current density, and (iv) peak voltage as functions of the volume ratio for doping with different ions. (v) Schematic of a TENG with ion gel deposits on the electrode surface, (vi) measured charge density with different ion concentrations at a pressure of 25 kPa, and (vii) output voltages of ion gel TENGs with different ion concentration as functions of applied pressure. Reprinted with permission from Ref. [41,42]. b- (i) Schematic and SEM image of porous PDMS with Au nanoparticles, (ii) porosity as a function of the DI water concentration (inset images are SEM images at 3%, 20%, and 50% DI water concentration), (iii) output performance of mesoporous AuNP/PDMS with different Au NP concentrations, and (iv) electrostatic potential of Au NP-embedded nanoporous TENG as a function of porosity calculated using the COMSOL multi-physics software. Inset shows the potential distributions in the pores of the mesoporous films. (v) Output voltage of porous PDMS-TENGs with different DI water concentrations. Reprinted with permission from Ref. [46]. c- (i) Schematic of the fabrication process of the hydrogel-TENG, (ii) illustration of interface formed between PDMS and hydrogel with benzophenone treatment, and (iii) voltage and (iv) current output performance of hydrogel-TENGs. Reprinted with permission from Ref. [48].

PDMS surface. These broken chains were highly susceptible to the absorption of H_2 or O_2 molecules from the atmosphere. The resulting oxidation of the PDMS surface decreased its charge density, which rapidly decreased the output voltage. In contrast, in the two-step plasma treatment, the broken molecular chains immediately bonded to reactive species, such as F, CF_3, CF_3^+, and O_2. In this case, the (C-F) branches significantly influenced the TENG output performance because of their higher electron affinities (Fig. 2c (iii)). The dependence of the output performance on the plasma exposure time was investigated. The optimal exposure time was 2 to 4 min. The output performance decreased at longer exposure times because of the reduced surface roughness.

2.3 Embedded Impurity Modification

Modification by impurity embedding can enhance the TENG performance through increasing the charge density on the surface and preventing triboelectric loss when nanomaterials are added to the contact layer. Impurity particles can play different roles in the TENG depending on the additive and base triboelectric materials. They can enhance the TENG performance by improving the dielectric properties and charge density.

The dielectric constant is an important parameter that affects the output performance[36-41]. Improving the dielectric properties of the materials is a simple approach for improving the TENG output performance. High-dielectric materials, such as SiO_2, TiO_2, $BaTiO_3$, and $SrTiO_3$, are preferred for modifying dielectric properties. Chen et al. modified the dielectric properties of PDMS by adding high-dielectric materials (Fig. 3a(i))[41]. The relative permittivity of the doped PMDS was investigated as a function of the doping concentration. The results are shown in Fig. 3a-(iii). Through the combined effects of enhanced permittivity and pore

production in the PDMS film in an optimized film containing 10% $SrTiO_3$ nanoparticles (approximately 100 nm in size) and 15% pores in volume, the charge density, open-circuit voltage, and power density of the film reached approximately 19 nC cm^{-2}, 338 V, and 6.47 W m^{-2}, respectively. This constitutes a power enhancement of more than five times compared with that of a nanogenerator based on a pure PDMS film. The effect of the nanoparticle concentration is shown in Fig. 3a (ii–iv). The optimal concentration was between 8% and 10% depending on the material. Significantly, the pores formed in/on the sponge PDMS film can effectively reduce its thickness and increase the contact effective area. The highest TENG performance was achieved at the optimal pore ratio of 15%.

Hwang et al. (2019) introduced an ion liquid TENG (iTENG) that included a TPU matrix and polymer ion pump (iTPU)[42]. Its operating mechanism is the migration of ions through the porous chain structures in the soft segments induced by mechanical contact (Fig. 3a (vi)). The highest output performance was exhibited by an iTPU film with 10 wt% ionic liquid, which provided the optimal condition for pressure to influence ion immigration and the resulting charge density. The voltage therefore increased with the pressure, as shown in Fig. 3a (vi) and (vii).

At the same time, TENG performance enhancement through the addition of conductive materials to triboelectric materials has also been demonstrated[43-46]. Chun et al. reported that the TENG performance was improved by adding Au nanoparticles[46]. They proposed that contact between the Au nanoparticles and PDMS inside the pores produced charges, which led to aligned dipoles that affected the surface potential energy of the porous films. The fabrication process of the TENG is illustrated in Fig. 3b-(i). PDMS and Au nanoparticle solutions were mixed, and the water was subsequently removed by applying heat. The TENG output performance was enhanced in the presence of the Au nanoparticles and increased with the Au nanoparticle concentration. The peak voltage of 150 V at 0.28 wt% Au nanoparticles was much higher than the 5 V produced by the pure PDMS film. Hwang et al. reported that adding metal oxides improved the output performance of TENGs[47]. They proposed that the metal oxide played a similar role to the Au nanoparticles by creating charges through contact between the metal oxide nanoparticles and PDMS inside the pores. This resulted in dipole alignment and a consequent increase in the dielectric constant of the film.

Soft and wearable TENG devices have attracted attention for potential applications in human sensors. Communication between humans and machines requires real-time response. Lee et al. developed a self-cleanable, transparent, and attachable ionic TENG (STAIC), which demonstrated sensitivity and electrical and optical stability, as a communication device for human sensors[48]. Fig. 3c-(i) shows the benzophenone treatment fabrication process of the STAICs. A hydrogel was covalently and robustly anchored to an elastomer (Fig. 3c(ii)). The output voltage and current increased by 24.5% and 17.5%, respectively, in the presence of (heptadecafluoro-1,1,2,2-tetrahydrodecyl) trichlorosilane (Fig. 3c-(ii)).

2.4 Interfacial Layer and TENG Structure Design

Performance enhancement in TENGs is limited by the electrification loss due to leakage current from the triboelectric material to the electrode, which is the largest source of charge loss. To address this issue, Park et al. suggested depositing a metal oxide layer between the triboelectric material and electrode[49]. As shown in Fig. 4a-(i), a deposited TiO_2 layer on the Al electrode called the electron blocking layer (EBL) not only separated positive and negative charges but also increased the polarization because of its high dielectric constant. Compared to a normal TENG, which generated a peak output voltage of approximately 50 V and peak output current of 2 μA, the output power was significantly increased in a TENG with a TiO_2 EBL, which produced a peak output voltage and current of approximately 272 V and 9.1 μA, respectively (Fig. 4a-(ii,iii)). The optimized TENG, which contained 100 nm-thick TiO_2, achieved the highest performance owing to the increased relative amount of oxygen vacancies.

Kim et al. significantly improved the output performance of a TENG by creating a molecular layer between the electrode and triboelectric material (Fig. 4b-(i))[49,50]. The molecular layer was created using the self-assembled monolayer (SAM) technique. The monolayer prevented opposite charges from recombining and increased the polarization. Fig. 4b-(ii) shows the power density as a function of load resistance for different monolayer types. The optimal performance was achieved in the TENG with an ABT monolayer because it generated the highest surface charge density.

Another strategy has been used in many studies to achieve a high power density. This strategy is optimal for designs that produce ultrahigh powers. Wu et al. demonstrated a power density of 10 MW/m^2 using a triboelectric generator that has a similar design to an opposite-charge-enhanced transistor [19]. Fig. 4c(i) shows two new TENG designs. In the OTC-TENG structure, the output current is controlled in each cycle using two left and right

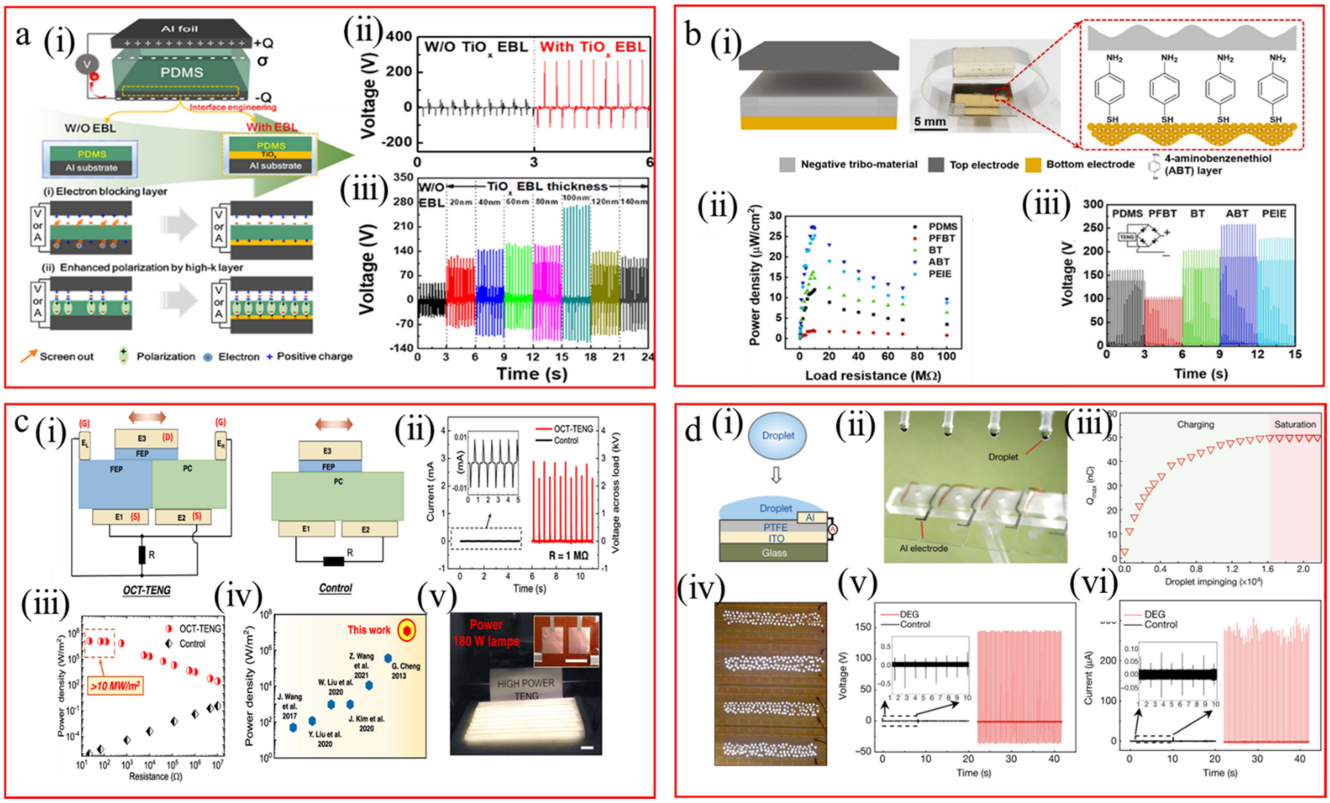

Fig. 4. a- (i) Schematic of the working principle of TENGs and role of multifunctional TiO_x EBL and output voltages of TENGs (ii) with/without TiO_x EBL and (iii) with different TiO_x EBL thicknesses. Reprinted with permission from Ref. [49]. b- (i) Schematic and photograph of the interfacial TENG. (ii) Power density and (iii) rectifying voltage output performance of interfacial TENGs with different negative tribo-materials. Reprinted with permission from Ref. [50]. c- (i) Schematic of the cross-section of the opposite-charge-enhanced transistor-like TENG (OCT-TENG) and conventional sliding mode TENG. (ii) Output current of the OCT-TENG and control TENG through 1 M resistance. (iii) Estimated power density of over 10 MW/m^2 achieved by OTC-TENG, (iv) comparison with other TENGs, and (v) demonstration of high output power from OTC-TENG using a 180 W lamp. Reprinted with permission from Ref. [19]. d- (i) Schematic and (ii) optical image of the droplet electricity generator (DEG). (iii) Amount of charge on the polytetrafluoroethylene (PTFE) surface increases gradually and eventually reach a stable value. (iv) Hundred LEDs were powered by one droplet on the DEG. Comparison of (v) voltage and (vi) current from DEG with a control device. Reprinted with permission from Ref. [51].

electrodes. Its output performance (Fig. 4c-(ii)) and estimated power density (Fig. 4c-(iii)) were improved significantly compared to those of other reported TENGs. It is clear that 10 MW/m^2 is the optimal value that has been reported thus far (Fig. 4c-(iv)). A single OTC-TENG can power a 180 W lamp (Fig. 4c-(v)), which is a highly practical application in everyday life.

Many researchers have attempted to improve the efficiency of raindrop generators through both physical and chemical modifications for the past decade. However, the raindrop generators typically had a low conversion value of 1%. In a significant study, a raindrop generator was fabricated by placing an electrode on the top triboelectric layer in direct contact with the droplet[51]

(Fig. 4d-(i,ii)). Importantly, a single drop produced a charge that approached 50 nC, voltage of 100 V, and current that exceeded 300 mA, as shown in Fig. 4d-(iii–vi). This opens significant prospects for applications of infinitive drain-drop energy[52-57].

3. CONCLUSIONS

The performance of TENGs can be enhanced by interfacial material engineering using a variety of physical, chemical, and biological methods. Despite being the simplest method, surface morphology modification can produce significant performance improvements. Chemical and biological methods are more complicated and have higher material selectivity but can produce large-scale output performance improvements. Many polymer treatments to enhance the output performance of TENGs, such as UV treatment, laser writing, plasma treatment, and the use of neutral beams, ion beam irradiation, wet chemical reactions, and

patterning, were discussed. In addition, new interlayer designs and operating mechanisms that resulted in significant enhancements of TENG performance were introduced. Enhancing output performance through a variety of modification approaches is important and promising for a variety of applications in green energy harvesting.

ACKNOWLEDGMENT

This study was supported by the Technology Innovation Program (20013794, Center for Composite Materials and Concurrent Design) funded by the Ministry of Trade, Industry, and Energy (MOTIE, Korea).

REFERENCES

[1] F. R. Fan, Z. Q. Tian, and Z. L. Wang, "Flexible triboelectric generator", *Nano Energy*, Vol. 1, No. 2, pp. 328-334, 2012.

[2] F. R. Fan, J. Luo, W. Tang, C. Li, C. Zhang, Z. Tian, and Z. L. Wang, "Highly transparent and flexible triboelectric nanogenerators: performance improvements and fundamental mechanisms", *J. Mater. Chem. A*, Vol. 2, No. 33, pp. 13219-13225, 2014.

[3] G. Zhu, B. Peng, J. Chen, Q. Jing, and Z. L. Wang, "Triboelectric nanogenerators as a new energy technology: from fundamentals, devices, to applications", *Nano Energy*, Vol. 14, pp. 126-138, 2015.

[4] Y. Zi, S. Niu, J. Wang, Z. Wen, W. Tang, and Z. L. Wang, "Standards and figure-of-merits for quantifying the performance of triboelectric nanogenerators", *Nat. Commun.*, Vol. 6, No. 1, pp. 1-8, 2015.

[5] Z. H. Lin, Y. Xie, Y. Yang, S. Wang, G. Zhu, and Z. L. Wang, "Enhanced triboelectric nanogenerators and triboelectric nanosensor using chemically modified TiO2 nanomaterials", *ACS Nano*, Vol. 7, No. 5, pp. 4554-4560, 2013.

[6] L. Zhang, B. Zhang, J. Chen, L. Jin, W. Deng, J. Tang, H. Zhang, H. Pan, M. Zhu, and W. Yang, "Lawn structured triboelectric nanogenerators for scavenging sweeping wind energy on rooftops", *Adv. Mater.*, Vol. 28, No. 8, pp. 1650-1656, 2016.

[7] Q. Liang, X. Yan, X. Liao, and Y. Zhang, "Integrated multiunit transparent triboelectric nanogenerator harvesting rain power for driving electronics", *Nano Energy*, Vol. 25, pp. 18-25, 2016,

[8] J. Chen, J. Yang, Z. Li, X. Fan, Y. Zi, Q. Jing, H. Guo, Z. Wen, K.C. Pradel, S. Niu, "Networks of triboelectric nanogenerators for harvesting water wave energy: a potential approach toward blue energy", ACS Nano, 9, pp. 3324-3331, 2015.

[9] J. Xiong, H. Luo, D. Gao, X. Zhou, P. Cui, G. Thangavel, K. Parida, and P. S. Lee, "Self-restoring, waterproof, tunable microstructural shape memory triboelectric nanogenerator for self-powered water temperature sensor", *Nano Energy*, Vol. 61, pp. 584-593, 2019.

[10] J. Chen, and Z. L. Wang, "Reviving vibration energy harvesting and self-powered sensing by a triboelectric nanogenerator", *Joule*, Vol. 1, No. 3, pp. 480-521, 2017.

[11] Z. Wu, W. Ding, Y. Dai, K. Dong, C. Wu, L. Zhang, Z. Lin, J. Cheng, and Z. L. Wang, "Self-powered multifunctional motion sensor enabled by magnetic-regulated triboelectric nanogenerator", *ACS Nano*, Vol. 12, No. 6, pp. 5726-5733, 2018.

[12] H. J. Ryoo, C. W. Lee, J. W. Han, W. Kim, and D. Choi, "A Triboelectric Nanogenerator Design for the Utilization of Multi-Axial Mechanical Energies in Human Motions", *J. Sens. Technol*., Vol. 29, No. 5, pp. 312-322, 2020.

[13] F. Yi, L. Lin, S. Niu, P. K. Yang, Z. Wang, J. Chen, Y. Zhou, Y. Zi, J. Wang, and Q. Liao, "Stretchable-rubber-based triboelectric nanogenerator and its application as self-powered body motion sensors", *Adv. Funct. Mater.*, Vol. 25, No. 24, pp. 3688-3696, 2015.

[14] Y. Jung and H. Cho, "Flexible Pressure Sensors Based on Three-dimensional Structure for High Sensitivity", *J. Sens. Technol.*, Vol. 31, No. 3, pp. 145-150, 2022.

[15] C. Cai, J. Mo, Y. Lu, N. Zhang, Z. Wu, S. Wang, and S. Nie, "Integration of a porous wood-based triboelectric nanogenerator and gas sensor for real-time wireless food-quality assessment", *Nano Energy*, Vol. 83, p. 105833, 2021.

[16] N. Rubab, and S. W. Kim, "Triboelectric Nanogenerators for Self-powered Sensors", *J. Sens. Technol.,* Vol. 31, No. 2, pp. 79-84, 2022.

[17] H. G. Menge, N. D. Huynh, H. J. Hwang, S. Han, D. Choi, and Y. T. Park, "Designable skin-like triboelectric nanogenerators using layer-by-layer self-assembled polymeric nanocomposites", *ACS Energy Lett.*, Vol. 6, No. 7, pp. 2451-2459, 2021.

[18] H. Park, J. Kim, and J. H. Lee, "Triboelectrification based Multifunctional Tactile Sensors", *J. Sens. Technol.*, Vol. 31, No. 3, pp. 139-144, 2022.

[19] H. Wu, S. Wang, Z. Wang, and Y. Zi, "Achieving ultrahigh instantaneous power density of 10 MW/m2 by leveraging the opposite-charge-enhanced transistor-like triboelectric nanogenerator (OCT-TENG)", *Nat. Commun.*, Vol. 12, No. 1, pp. 1-8, 2021.

[20] B. Dudem, N. D. Huynh, W. Kim, D. H. Kim, H. J. Hwang, D. Choi, and J. S. Yu, "Nanopillar-array architectured PDMS-based triboelectric nanogenerator integrated with a windmill model for effective wind energy harvesting", *Nano Energy*, Vol. 42, pp. 269-281, 2017.

[21] F. R. Fan, L. Lin, G. Zhu, W. Wu, R. Zhang, and Z. L. Wang, "Transparent triboelectric nanogenerators and self-powered pressure sensors based on micropatterned plastic films", *Nano Lett.,* Vol. 12, No. 6, pp. 3109-3114, 2012.

[22] J. Huang, X. Fu, G. Liu, S. Xu, X. Li, C. Zhang, and L. Jiang, "Micro/nano-structures-enhanced triboelectric nanogenerators by femtosecond laser direct writing", *Nano Energy*, Vol. 62, pp. 638-644, 2019.

[23] H. J. Kim, J. H. Kim, K. W. Jun, J. H. Kim, W. C. Seung,

O. H. Kwon, J. Y. Park, S. W. Kim, and I. K. Oh, "Silk nanofiber-networked bio-triboelectric generator: silk bio-TEG", *Adv. Energy Mater*, Vol. 6, No. 8, p. 1502329, 2016.

[24] T. Huang, M. Lu, H. Yu, Q. Zhang, H. Wang, and M. Zhu, "Enhanced power output of a triboelectric nanogenerator composed of electrospun nanofiber mats doped with graphene oxide", *Sci. Rep.*, Vol. 5, No. 1, pp. 1-8, 2015.

[25] G. Q. Gu, C. B. Han, C. X. Lu, C. He, T. Jiang, Z. L. Gao, C. J. Li, and Z. L. Wang, "Triboelectric nanogenerator enhanced nanofiber air filters for efficient particulate matter removal", *ACS Nano*, Vol. 11, No. 6, pp. 6211-6217, 2017.

[26] A. Yar, A. Karabiber, A. Ozen, F. Ozel, and S. Coskun, "Flexible nanofiber based triboelectric nanogenerators with high power conversion", *Renew. Energy*, Vol. 162, pp. 1428-1437, 2020.

[27] X. Zhang, S. Lv, X. Lu, H. Yu, T. Huang, Q. Zhang, and M. Zhu, "Synergistic enhancement of coaxial nanofiber-based triboelectric nanogenerator through dielectric and dispersity modulation", *Nano Energy*, Vol. 75, p. 104894, 2020.

[28] G. Zhu, Z. H. Lin, Q. Jing, P. Bai, C. Pan, Y. Yang, Y. Zhou, and Z. L. Wang, "Toward large-scale energy harvesting by a nanoparticle-enhanced triboelectric nanogenerator", *Nano Lett.,* Vol. 13, No. 2, pp. 847-853, 2013.

[29] Y. Y. Ba, J. F. Bao, H. T. Deng, Z. Y. Wang, X. W. Li, T. Gong, W. Huang, and X. S. Zhang, "Single-Layer Triboelectric Nanogenerators Based on Ion-Doped Natural Nanofibrils", *ACS Appl. Mater. Interfaces*, Vol. 12, No. 38, pp. 42859-42867, 2020.

[30] J. W. Lee, S. Jung, J. Jo, G. H. Han, D. M. Lee, J. Oh, H. J. Hwang, D. Choi, S. W. Kim, and J. H. Lee, "Sustainable highly charged C 60-functionalized polyimide in a non-contact mode triboelectric nanogenerator", *Energy Environ. Sci*., Vol. 14, No. 2, pp. 1004-1015, 2021.

[31] W. Kim, T. Okada, H. W. Park, J. Kim, S. Kim, S. W. Kim, S. Samukawa, and D. Choi, "Surface modification of triboelectric materials by neutral beams", *J. Mater. Chem. A,* Vol. 7, No. 43, pp. 25066-25077, 2019.

[32] G. G. Cheng, S. Y. Jiang, K. Li, Z. Q. Zhang, Y. Wang, N. Y. Yuan, J. N. Ding, and W. Zhang, "Effect of argon plasma treatment on the output performance of triboelectric nanogenerator", *Appl. Surf. Sci*., Vol. 412, pp. 350-356, 2017.

[33] X. Cheng, B. Meng, X. Chen, M. Han, H. Chen, Z. Su, M. Shi, and H. Zhang, "Single-step fluorocarbon plasma treatment-induced wrinkle structure for high-performance triboelectric nanogenerator", *Small,* Vol. 12, No. 2, pp.229-236, 2016.

[34] X. Cheng, L. Miao, Z. Su, H. Chen, Y. Song, X. Chen, and H. Zhang, "Controlled fabrication of nanoscale wrinkle structure by fluorocarbon plasma for highly transparent triboelectric nanogenerator", *Microsyst. Nanoeng.*, Vol. 3, No. 1, pp. 1-9, 2017.

[35] C. Lee, S. Yang, D. Choi, W. Kim, J. Kim, and J. Hong, "Chemically surface-engineered polydimethylsiloxane layer via plasma treatment for advancing textile-based triboelectric nanogenerators", *Nano Energy*, Vol. 57, pp. 353-362, 2019.

[36] R. Wen, J. Guo, A. Yu, K. Zhang, J. Kou, Y. Zhu, Y. Zhang, B. W. Li, and J. Zhai, "Remarkably enhanced triboelectric nanogenerator based on flexible and transparent monolayer titania nanocomposite", *Nano Energy*, Vol. 50, pp. 140-147, 2018.

[37] S. Gao, R. Wang, C. Ma, Z. Chen, Y. Wang, M. Wu, Z. Tang, N. Bao, D. Ding, and W. Wu, "Wearable high-dielectric-constant polymers with core–shell liquid metal inclusions for biomechanical energy harvesting and a self-powered user interface", *J. Mater. Chem. A*, Vol. 7, No. 12, pp. 7109-7117, 2019.

[38] Y. Yu, Z. Li, Y. Wang, S. Gong, and X. Wang, "Sequential infiltration synthesis of doped polymer films with tunable electrical properties for efficient triboelectric nanogenerator development", *Adv. Mater*., Vol. 27, No. 33, pp. 4938-4944, 2015.

[39] G. Suo, Y. Yu, Z. Zhang, S. Wang, P. Zhao, J. Li, and X. Wang, "Piezoelectric and triboelectric dual effects in mechanical-energy harvesting using a TiO3/polydimethylsiloxane composite film", *ACS Appl. Mater. Interfaces*, Vol. 8, No. 50, pp. 34335-34341, 2016.

[40] Y. H. Kwon, S. H. Shin, Y. H. Kim, J. Y. Jung, M. H. Lee, and J. Nah, "Triboelectric contact surface charge modulation and piezoelectric charge inducement using polarized composite thin film for performance enhancement of triboelectric generators", *Nano Energy*, Vol. 25, pp. 225-231, 2016.

[41] J. Chen, H. Guo, X. He, G. Liu, Y. Xi, H. Shi, and C. Hu, "Enhancing Performance of Triboelectric Nanogenerator by Filling High Dielectric Nanoparticles into Sponge PDMS Film", *ACS Appl. Mater. Interfaces*, Vol. 8, No. 1, pp. 736-744, 2016.

[42] H. J. Hwang, J. S. Kim, W. Kim, H. Park, D. Bhatia, E. Jee, Y. S. Chung, D. H. Kim, and D. Choi, "An ultra-mechanosensitive visco-poroelastic polymer ion pump for continuous self-powering kinematic triboelectric nanogenerators", *Adv. Energy Mater.*, Vol. 9, No. 17, p. 1803786, 2019.

[43] X. Xia, J. Chen, G. Liu, M.S. Javed, X. Wang, and C. Hu, "Aligning graphene sheets in PDMS for improving output performance of triboelectric nanogenerator", Carbon, Vol. 111, pp. 569-576, 2017.

[44] S. Bayan, S. Pal, and S. K. Ray, "Interface engineered silver nanoparticles decorated g-C3N4 nanosheets for textile based triboelectric nanogenerators as wearable power sources", *Nano Energy*, Vol. 94, p. 106928, 2022.

[45] S. Kuntharin, V. Harnchana, A. Klamchuen, K. Sinthiptharakoon, P. Thongbai, V. Amornkitbamrung, P. Chindaprasirt, "Boosting the Power Output of a Cement-Based Triboelectric Nanogenerator by Enhancing Dielectric Polarization with Highly Dispersed Carbon Black Nanoparticles toward Large-Scale Energy Harvesting from Human Footsteps", ACS Sustain. Chem. Eng., Vol. 10, No. 14, pp. 4588-4598, 2022.

[46] J. Chun, J. W. Kim, W. S. Jung, C. Y. Kang, S. W. Kim, Z. L. Wang, and J. M. Baik, "Mesoporous pores impregnated with Au nanoparticles as effective dielectrics for enhancing triboelectric nanogenerator performance in harsh environments", *Energy Environ. Sci.*, Vol. 8, No. 10, pp. 3006-3012, 2015.

[47] H. J. Hwang, Y. Lee, C. Lee, Y. Nam, J. Park, D. Choi, and

D. Kim, "Mesoporous highly-deformable composite polymer for a gapless triboelectric nanogenerator via a one-step metal oxidation process", *Micromachines*, Vol. 9, No. 12, pp. 656(1)-656(11), 2018.

[48] Y. Lee, S. H. Cha, Y. W. Kim, D. Choi, and J. Y. Sun, "Transparent and attachable ionic communicators based on self-cleanable triboelectric nanogenerators", *Nat. Commun.*, Vol. 9. No. 1, pp. 1-8, 2018.

[49] H. W. Park, N. D. Huynh, W. Kim, C. Lee, Y. Nam, S. Lee, K. B. Chung, and D. Choi, "Electron blocking layer-based interfacial design for highly-enhanced triboelectric nanogenerators", *Nano Energy*, Vol. 50, pp. 9-15, 2018.

[50] W. Kim, J. H. Park, H. J. Hwang, Y. S. Rim, and D. Choi, "Interfacial molecular engineering for enhanced polarization of negative tribo-materials", *Nano Energy*, Vol. 96, p. 107110, 2022.

[51] W. Xu, H. Zheng, Y. Liu, X. Zhou, C. Zhang, Y. Song, X. Deng, M. Leung, Z. Yang, and R. X. Xu, "A droplet-based electricity generator with high instantaneous power density", *Nature*, Vol. 578, No. 7795, pp. 392-396, 2020.

[52] A. Riaud, C. Wang, J. Zhou, W. Xu, Z. Wang, "Hydrodynamic constraints on the energy efficiency of droplet electricity generators", *Microsyst. Nanoeng*, Vol. 7, No. 1, pp. 1-10, 2021.

[53] L. Wang, Y. Song, W. Xu, W. Li, Y. Jin, S. Gao, S. Yang, C. Wu, S. Wang, and Z. Wang, "Harvesting energy from high-frequency impinging water droplets by a droplet-based electricity generator", EcoMat, Vol. 3, No. 4, pp. e12116(1)-e12116(9), 2021.

[54] X. Wang, S. Fang, J. Tan, T. Hu, W. Chu, J. Yin, J. Zhou, and W. Guo, "Dynamics for droplet-based electricity generators", *Nano Energy*, Vol. 80, p. 105558, 2021.

[55] Q. Zhang, Y. Li, H. Cai, M. Yao, H. Zhang, L. Guo, Z. Lv, M. Li, X. Lu, and C. Ren, "A Single-Droplet Electricity Generator Achieves an Ultrahigh Output Over 100 V Without Pre-Charging", *Adv. Mater.*, Vol. 33, No. 51, p. 2105761, 2021.

[56] J. Dong, C. Xu, L. Zhu, X. Zhao, H. Zhou, H. Liu, G. Xu, G. Wang, G. Zhou, and Q. Zeng, "A high voltage direct current droplet-based electricity generator inspired by thunderbolts", *Nano Energy*, Vol. 90, p. 106567, 2021.

[57] N. Zhang, H. Gu, K. Lu, S. Ye, W. Xu, H. Zheng, Y. Song, C. Liu, J. Jiao, and Z. Wang, "A universal single electrode droplet-based electricity generator (SE-DEG) for water kinetic energy harvesting", *Nano Energy*, Vol. 82, p. 105735, 2021.